Available online at www.sciencedirect.com
ScienceDirect
Ceramics International 37 (2011) 3203–3209
CERAMICS INTERNATIONAL
www.elsevier.com/locate/ceramint

Preparation and characterization of nanometer-sized $(Pb_{1-x},Ba_x)TiO_3$ powders using acetylacetone as a chelating agent in a non-aqueous sol–gel process

Hong Zhu [a], Zhijun Guo [b], Wein-Duo Yang [c,*], Wein-Feng Chang [c], Cheng-Chin Wang [c]

[a] *Institute of Modern Catalysis, Department of Organic Chemistry, State key Laboratory of Chemical Resource Engineering, Beijing University of Chemical Technology, Beijing 100029, PR China*
[b] *School of Science, Beijing Jiaotong University, Beijing 100044, PR China*
[c] *Department of Chemical and Materials Engineering, National Kaohsiung University of Applied Sciences, Kaohsiung 807, Taiwan*

Received 30 August 2010; received in revised form 18 January 2011; accepted 22 March 2011
Available online 27 May 2011

Abstract

Nanometer-sized lead barium titanate ($Pb_{1-x}Ba_xTiO_3$, PB_xT) powders were prepared by a non-aqueous sol–gel process using lead acetate, barium acetate, and titanium isopropoxide as precursors and ethylene glycol as the solvent. In this procedure, Ti-isopropoxide was chelated with acetylacetone. The samples were characterized by Fourier transform infrared spectroscopy (FTIR), Raman spectroscopy, thermogravimetric analysis/differential thermal analysis (TGA/DTA), X-ray diffraction (XRD), scanning electron microscopy (SEM) and Brunauer–Emmett–Teller (BET) specific surface area analysis. The results indicate that perovskite PB_xT phases were obtained by heat treatment at 450 °C for 5 h, and a pure perovskite was examined at 600 °C. The average particle sizes of perovskite PB_xT powders calcined at 600 °C were approximately about 40–80 nm, and BET analysis showed that the surface areas of the powders obtained at 600 °C were approximately 6–16 m^2/g. In addition, the phase transition from the tetragonal ferroelectric phase to the cubic paraelectric phase occurred in a range of approximately $0.6 < x < 0.8$.

Keywords: Nanometer-sized; Lead barium titanate; Non-aqueous; Sol–gel process

1. Introduction

The sol–gel method involving hydrolysis and polycondensation, gelation, aging, drying and heat treatment results in homogeneous distributed particles with high purity and controlled chemical composition [1,2]. It is important that the sol–gel synthesis is carried out at a low temperature.

Solid solutions of lead barium titanate with excellent dielectric [3], piezoelectric [4], pyroelectric [5], ferroelectric [6] and optical properties [7] are used in many electronic and optical devices, including non-volatile random access memories, infrared sensors and actuators. The compatibility of the starting materials is important to form a stable precursor solution in the multicomponent system.

Ti alkoxides are more moisture-sensitive, and therefore, some chemical agents are added to stabilize the Ti precursor [8–10]. Using acetylacetone as a chelating agent with metal alkoxide can affect the hydrolysis of the starting materials to produce new precursors [6,11]. However, the metal-organic precursor chelated with acetylacetone is no longer moisture-sensitive [12]. In our previous work, acetylacetone-chelated Ti isopropoxide at a molar ratio of 1:4 produced modified metal-organic precursors with better uniformity, and the PBT powder obtained possessed better mechanical properties and lower synthesis temperature [13].

Some research results on $Pb_{1-x}Ba_xTiO_3$ thin films, powders and ceramics by sol–gel processing are available in the literature [14,15,12]. The $Pb_{1-x}Ba_xTiO_3$ system has not been thoroughly studied. In this paper, $Pb_{1-x}Ba_xTiO_3$ powders were prepared by a non-aqueous sol–gel route and characterized in detail. Moisture-free $Pb_{1-x}Ba_xTiO_3$ sols were obtained by mixing Ti isopropoxide chelated with acetylacetone and an ethylene glycol solution dissolved with lead acetate tri-hydrate

* Corresponding author.
E-mail address: ywd@cc.kuas.edu.tw (W.-D. Yang).

0272-8842/$36.00 © 2011 Published by Elsevier Ltd and Techna Group S.r.l.
doi:10.1016/j.ceramint.2011.05.090

and barium acetate for a non-aqueous system. In the process, $Pb_{1-x}Ba_xTiO_3$ sol at various compositions were heat-treated, and the structural transformation, crystal structure and surface morphology of the lead barium titanate ceramic powders were studied by FTIR, Raman, TGA/TDA, XRD, SEM, and BET.

2. Experimental

Lead acetate trihydrate (Riedel-de Haën) and barium acetate (Baker) were, respectively, dissolved in ethylene glycol (Riedel-de Haën) in a refluxing condenser at 120–150 °C, respectively, to remove residual water. Titanium isopropoxide (Acros Organics) was chelated with acetylacetone (Fluka) at a molar ratio of 1:4 and dissolved in ethylene glycol at 120 °C.

Under electromagnetic agitation, precursor solution containing Pb, Ba, and Ti was obtained by mixing the acetate dissolved in ethylene glycol and Ti isopropoxide chelated with acetylacetone by refluxing at 120 °C. A dried gel was obtained after heating in an oven at 120 °C. In the same time, the organic solvent or the low-boiling point by-products formed during the sol–gel process were removed. Then, the dried gels were pulverized in an agate mortar and heat-treated at different temperatures from 200 to 600 °C for 5 h. The scheme for preparing $Pb_{1-x}Ba_xTiO_3$ from the sol–gel to the powders is outlined in Fig. 1.

The dried gel and powder were studied by FTIR, Raman spectroscopy, and TGA/TDA. The gel and powders were examined by FTIR (FTS165 WIN-IR spectrometer) with a resolution of 4 cm^{-1} over the wavenumber range of 4000–400 cm^{-1}. The composition and structure of the gels and powders were probed by Raman spectroscopy (JOBIN YVON T64000) with a resolution of 1.3 cm^{-1} over the wavenumber range 100–1600 cm^{-1}. The thermal decomposition characteristics of the dried gel were studied using a thermogravimetric

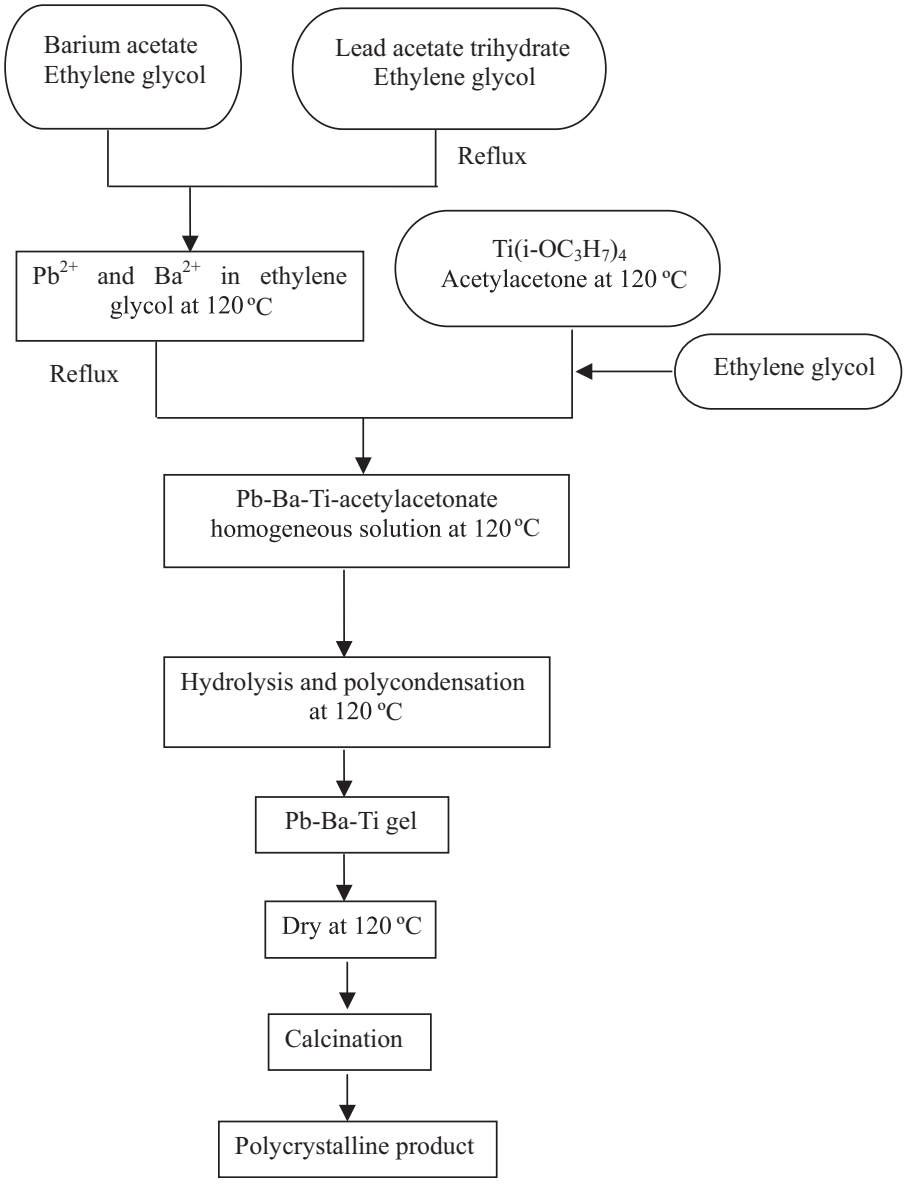

Fig. 1. Flow chart for the preparation of $Pb_{1-x}Ba_xTiO_3$ by sol–gel method.

analysis/differential scanning calorimeter (Du Pont SDT2960) at a constant heating rate of 5 °C/min from room temperature to 800 °C in air. Powders were examined by X-ray diffraction (XRD) (RIGAKU, Rint-2000) with a scanning step of 4°/min and the range of 2θ angles from 20° to 80°. The samples were also characterized using field-emission scanning electron microscopy (FESEM) and Brunauer–Emmett–Teller (BET) specific surface area analysis.

3. Results and discussion

3.1. Chemical and physical properties of Pb–Ba–Ti-gels

Fig. 2 shows the FTIR spectra of PB_xT dried gels. As seen in all of the FTIR spectra, the broad band at around 3400 cm^{-1} corresponds to the ν(O–H) of hydroxyl groups of residual water or ethylene glycol in the dried gel. The vibration frequencies of C–H in methylene and methyl group appear near 3000–2800 cm^{-1}. The two absorption bands at 1560 and 1420 cm^{-1} are ascribed to $\nu_{asym}(COO^-)$ and $\nu_{sym}(COO^-)$ of the acetyl groups, revealing that acetyl groups exist in the crosslinked networks of the dried gel [16]. The two peaks represent the characteristic adsorption wavelengths of the crosslinked networks obtained by Ti chelated with acetylacetone. The 1020 cm^{-1} peak corresponding to the Ti–O–C vibration of isopropoxide groups bonded to Ti indicates that the hydrolysis of Ti isopropoxide is not complete [17]. In addition, the absorption curve at 800–400 cm^{-1} is smooth, indicating the formation of Ba–O, Pb–O, and Ti–O.

The vibration bands frequencies 1720–1200 cm^{-1} were almost similar, revealing that the Ti isopropoxide chelated with acetylacetone can hinder a formation of complexes by reacting with moisture. Upon increasing the barium content, the vibration of Ti–C–O at 1020 cm^{-1} was weakened, which shows that the hydrolysis reaction was significantly strengthened.

Fig. 3 shows the Raman spectra of PB_xT gel as a function of x. In the Raman spectra, there are four Raman bands at 862, 1088, 1266 and 1464 cm^{-1}. The peak at 862 cm^{-1} is assigned to  of isopropanol, a by-product obtained from the polycondensation reaction, indicating that hydrolysis had occurred and the existence of a crosslinked network. The Raman shift at 1088 cm^{-1} corresponded to C–O of ethylene glycol in the gel [18]. The Raman band of C–O in acetate occurred at 1088 cm^{-1}, and the band at 1464 cm^{-1} may be ascribed to $\nu_{sym}(COO^-)$ the of acetyl groups in acetate, which indicates that the acetyl groups existed as carboxyl groups in the crosslinked networks after the PBT gel formation. The peak at 635 cm^{-1} is assigned to Ti–O. The broad and flat band from 500 to 600 cm^{-1} is due to $Ti–O^-$ in $(Ti–O^-)\ M^{2+}$.

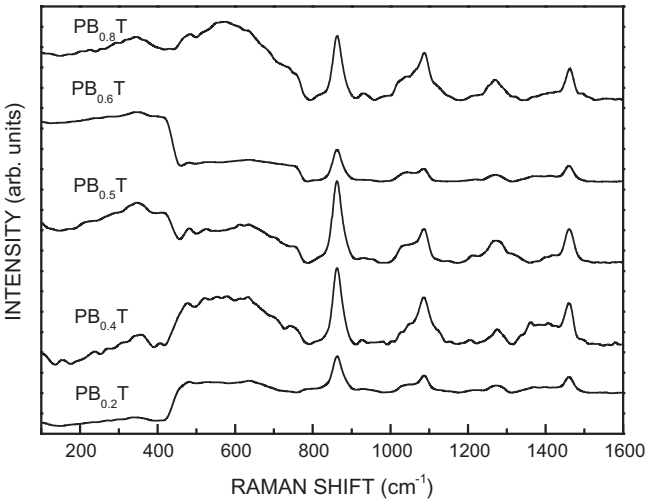

Fig. 3. Raman spectra of PB_xT gel as a function of x.

With increasing amounts of barium, the broad and flat band from 500 to 600 cm^{-1} changed to a weak peak, which indicates that M–O–M was incompletely formed from M–OR. Compared to the FTIR spectra, the Raman spectra also showed that the hydrolysis reaction was significantly strengthened with increasing barium content in PB_xT.

A thermogravimetric analyzer and differential thermal analyzer were used to analyze the PBT gel dried at 120 °C at a constant heating rate of 5 °C/min. The DTA/TGA curves for the dried $PB_{0.4}T$ gel are shown in Fig. 4. In Fig. 4, two major steps of weight loss are observed in the TGA curve over the

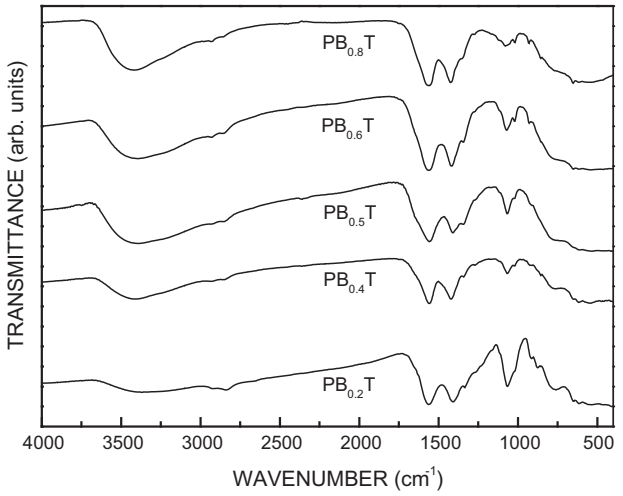

Fig. 2. FTIR spectra of PB_xT dried gel as a function of x.

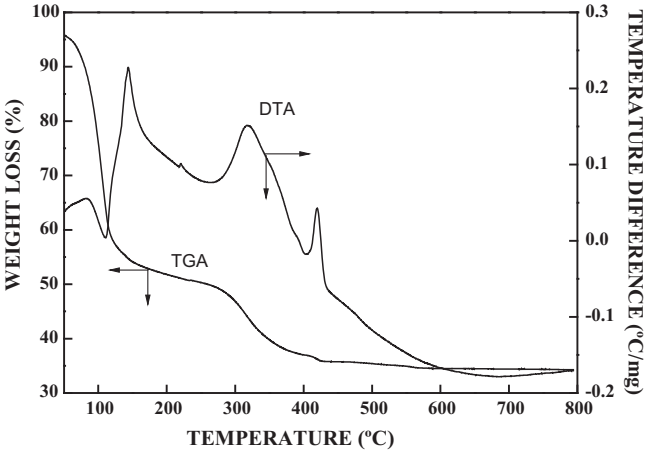

Fig. 4. TGA/DTA curves of the dried $PB_{0.4}T$ gel at a constant heating rate of 5 °C/min.

temperature range 50–400 °C. The first weight loss is below 150 °C, and subsequent weight loss occurs over the temperature range 250–400 °C. The curve is flat beyond 450 °C, which shows that the thermal decomposition was almost complete. In the DTA/TGA curves, there is an endothermal peak at 110 °C and three exothermal peaks at 145, 318 and 419 °C. However, the endothermal peak at 110 °C is due to the evaporation of residual water and low boiling-point organics in the gel as the temperature is increased. The exothermal peak at 145 °C is attributed to the cracking of the low-molecular-weight organic. According to the literature, the pyrolysis temperature range of acetate is near 320–360 °C, and the exothermal peak at 318 °C is thus due to the pyrolysis of the acetate, during which the chemical bonding in the gel changes to that of polymer. The exothermal peak at 419 °C is due to the cracking of the polymer organic or the formation of an inorganic substance. The curves are flat beyond 450 °C, which indicates that the pyrolysis of most of the organics was complete, and no distinct weight loss was observed. With increasing temperature, the small exothermal peaks were due to the pyrolysis of metal organics. A distinct weight loss at approximately 500–600 °C is attributed to the pyrolysis of the organic Ti-chelating agent. No weight loss was observed beyond 600 °C.

The DTA of PB_xT gel at approximately 200–400 °C was also performed. With increasing barium content, the temperature of the exothermal peak decreased. Based on the results obtained from the FTIR and Raman spectra, this indicates that the hydrolysis reaction was significantly strengthened with increasing barium content in PB_xT. With a relatively higher fraction of Ba, a gel with a less crosslinking network was formed; therefore, it required a lower energy to crack during calcination. This could be the reason that the temperature of the exothermal peak was lower with increasing barium content in the dried gel.

3.2. Characterization of $(Pb_{1-x},Ba_x)TiO_3$ powders

Fig. 5 shows the FTIR spectra of the $PB_{0.4}T$ dried gel heat-treated at various temperatures for 5 h. The bands at 3400 cm^{-1} correspond to ν(O–H), and that at 3000–2800 cm^{-1} is assigned to C–H of methylene. The methyl peaks are weaker and disappear with increasing temperature. The organics in the $PB_{0.4}T$ gel cracked and disappeared upon increasing the heat-treatment temperature. After increasing the heat-treatment temperature, the sharp peaks at 1560 and 1420 cm^{-1} became flat and weaker, then merged into a peak at 1440 cm^{-1}. The peak at 1440 cm^{-1}, corresponding to the vibration of COO^-, is sharper at 450 °C because of the formation of carbonate in the heat treatment process [19]. The peak at 1020 cm^{-1} was not observed at temperatures above 450 °C, revealing that C–O was cracked and that the organics were removed.

The organics in the PBT gel completely disappeared, and crystallization of the PBT occurred at 450 °C. The broad and flat bands at approximately 400–800 cm^{-1} corresponded to M–O in the metal oxide and then became sharp and split into two peaks at 450 cm^{-1} and 600 cm^{-1}. The characteristic absorption peaks at 450 cm^{-1} and 600 cm^{-1} are assigned to the stretching vibration and bending vibration of TiO_6 octahedrons, respectively [20]. The data reveals the change from amorphous TiO_2 to crystalline TiO_6 octahedrons with a perovskite structure. The characteristic absorption peaks of the M–O stretching vibration in the TiO_6 octahedrons were observed at 450 °C and became more intense with increasing temperature. The XRD data indicated that PBT perovskite crystallization occurred at approximately 400–450 °C and that the crystallinity increased with temperature. A high-purity PBT perovskite phase was ultimately formed and only trace amounts of intermediate carbonate impurity phases were obtained.

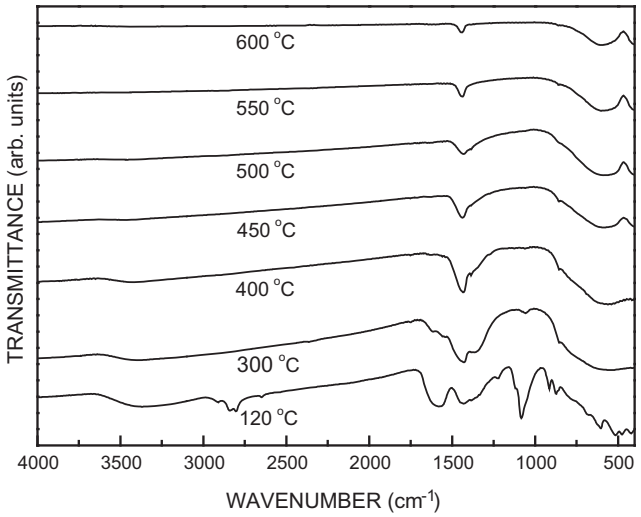

Fig. 5. FTIR spectra of the $PB_{0.4}T$ gel powders heat-treated at various temperatures: 120, 300, 400, 450, 500, 550, and 600 °C for 5 h.

The dried gel was also examined by XRD, which revealed that the gels heat-treated at temperatures below 450 °C were almost completely amorphous. There were some small peaks that indicated the occurrence of perovskite structures. The peaks with impurity phase diffraction peaks show that the pyrochlore phase and the perovskite phase existed in the calcined powder. The pyrochlore phase diffraction peaks became weak, and the perovskite phase diffraction peaks became strong, which indicate that the pyrochlore phase was the metaphase between the PBT gel and the perovskite structure. The fraction of the perovskite phase increased, and the lattice structure became more regular with increasing temperature. Only a single phase (perovskite) was observed at 600 °C, which is in agreement with the FTIR and TGA/DTA data.

The XRD patterns present in Fig. 6 show PB_xT powders with various x-values heat-treated at 600 °C. Both $PB_{0.2}T$ and $PB_{0.8}T$ powders in the perovskite phases indicated the replacement of Pb in the lattice without any second phase. At $x = 0.2$, the diffraction peaks associated with (0 0 1) and (1 0 0) reflections near 21–23° and (1 0 1) and (1 1 0) reflections near 31–33° were attributed to the degenerate state. At $x > 0.4$, the asymmetric diffraction peaks corresponding to (1 0 0) and (1 1 0) reflections occurred, which shows that crystallization transformed PBT from the club phase to the pseudo-cubic phase. The XRD peak at 44–47° of PB_xT shows that the single

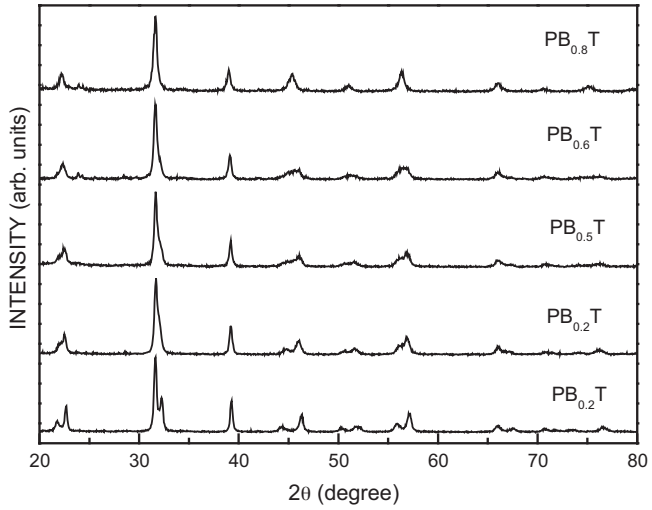

Fig. 6. XRD patterns of the PB_xT powders heat-treated at 600 °C.

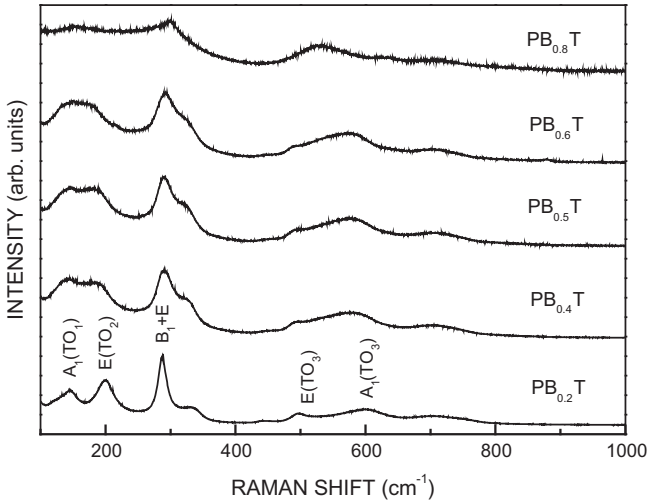

Fig. 8. Raman spectra of PB_xT powders heat-treated at 600 °C as a function of x.

peak obtained from the splitting peaks, which indicates that the PBT phase changed from the cubic phase to the tetragonal phase (not shown).

Fig. 7 shows the lattice parameters at which the tetragonality (c/a) of PB_xT powders was obtained at 600 °C. The ionic radius of Ba^{2+} is larger than that of Pb^{2+}. With increasing x, the "a" axis value increases and the "c" axis value decreases, resulting in a decrease in the c/a ratio. The c/a ratio was approximately 1 for $x \approx 0.8$. These results indicate that the PBT phase changes from the cubic phase to the tetragonal phase upon increasing x, and the composition range of cubic/tetragonal phase boundary was approximately $0.6 < x < 0.8$.

The Raman spectra of the gels were also observed at <450 °C; they indicate that the lattice vibration modes of the PBT powders were disordered and that the lattice structure was amorphous. With increasing temperature, the vibrational mode became significant and the intensity of the Raman spectra became strong, which indicates that the crystallization of $PB_{0.4}T$ powder was established gradually, in agreement with the XRD data discussed previously. A high-purity $PB_{0.4}T$ powder was obtained at 600 °C.

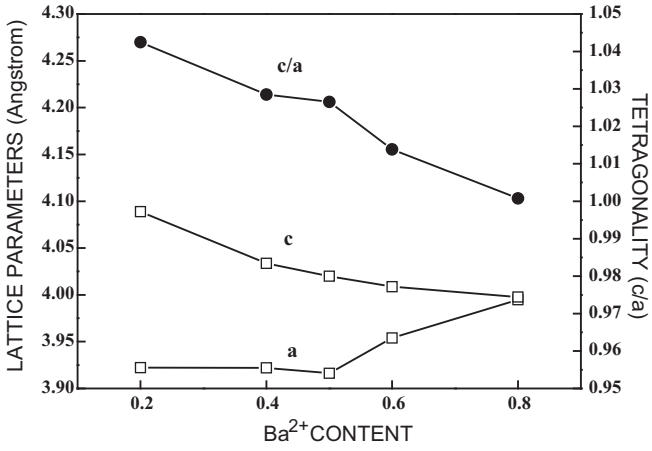

Fig. 7. Lattice variations in PBT powders as a function of Ba^{2+}.

Fig. 8 shows the Raman spectra of PB_xT powders as a function of x. In this figure, the $E(TO_2)$ (201 cm^{-1}) and the $A(TO_3)$ (600 cm^{-1}) phonon modes observed in the PB_xT powders are shifted gradually toward low frequencies upon increasing the barium content, and then merged into $A1(TO_1)$ (144 cm^{-1}) and $E(TO_3)$(497 cm^{-1}) at 148 and 456 cm^{-1}, respectively [21]. The band at 288 cm^{-1} became weak with increasing barium content and disappeared at $x > 0.6$. The intensity of the B_1 and E phonon modes became weak upon increasing barium content and disappeared at $x = 0.8$, which indicates, that the $PB_{0.8}T$ powder was paraelectric. Thus, the phase transition from the tetragonal ferroelectric to the cubic paraelectric phase occurred in a range of approximately $0.6 < x < 0.8$.

Fig. 9 shows SEM micrographs of the PB_xT powders as a function of x. The SEM micrographs show that the PB_xT powders were nanometer-sized and aggregated. The average particle size of the $PB_{0.2}T$ powders was approximately 80–100 nm, and that of the $PB_{0.8}T$ was about 40–60 nm. Under the same conditions, the average particle size of the PB_xT powders became small upon increasing x. With increasing barium content, the phase of the PBT powders transformed from the tetragonal phase to the cubic phase, which implies a decrease in the particle size associated with the phase change. The specific surface areas of the PBT powders were determined by BET, as listed in Table 1. As seen in this table, the specific surface areas increased from 6.3 m^2/g to 16.6 m^2/g upon increasing the barium content, which correlates well with the SEM results.

Table 1
The specific areas and the particle sizes of the PBT powders.

PB_xT	Specific surface area (m^2/g)	Particle sizes (nm)
$x = 0.2$	6.228	80–100
$x = 0.4$	6.514	70–90
$x = 0.5$	10.484	60–80
$x = 0.6$	13.708	50–70
$x = 0.8$	16.592	40–60

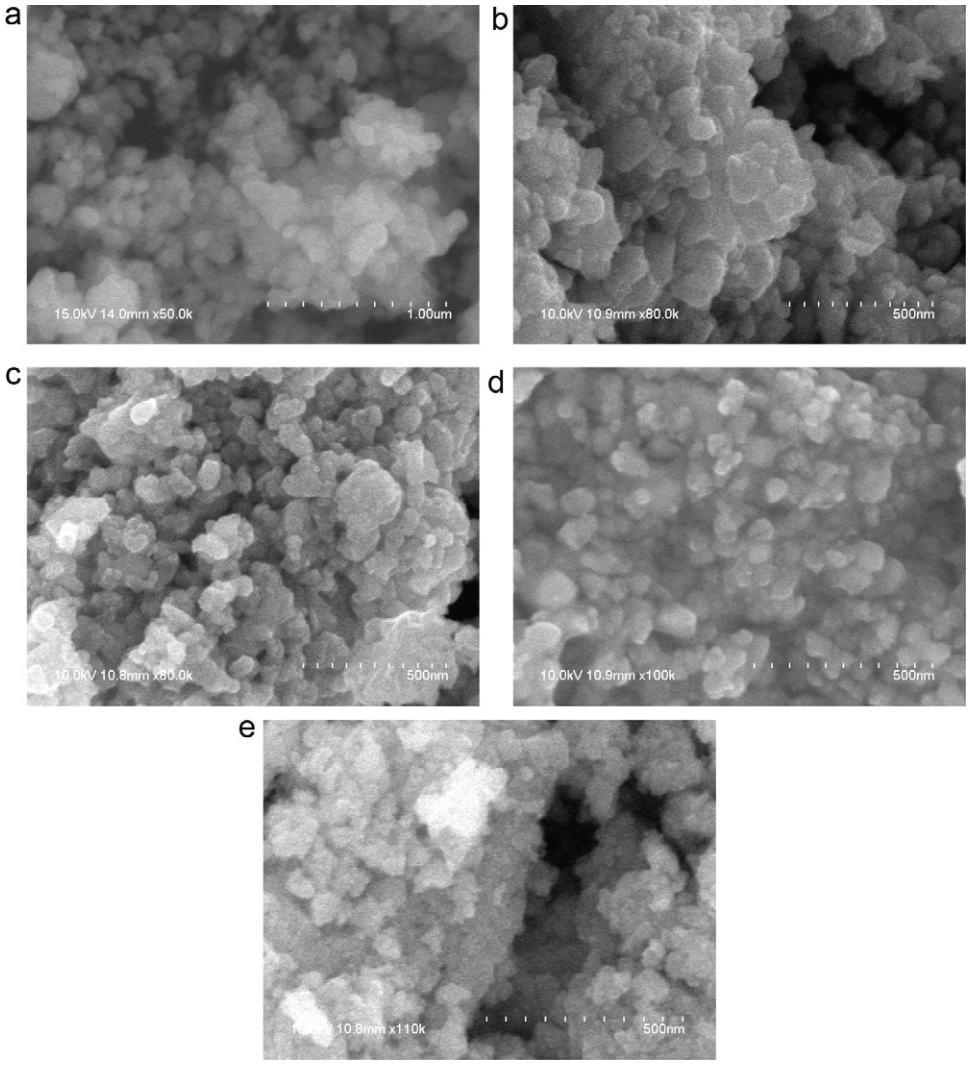

Fig. 9. The SEM micrographs of the PB_xT powders as a function of x: (a) $x = 0.2$, (b) $x = 0.4$, (c) $x = 0.5$, (d) $x = 0.6$, and (e) $x = 0.8$.

4. Conclusions

Nanometer-sized $Pb_{1-x}Ba_xTiO_3$ powders were prepared by a non-aqueous sol–gel process with acetylacetone as a chelating agent and ethylene glycol as a solvent. In the sol–gel process, the hydrolysis reaction was significantly strengthened and the polycondensation reaction was weakened upon increasing the barium content, which crosslinked the network gel cracked at lower temperatures. The crystallization of the $PB_{0.4}T$ perovskite structure occurred at temperatures as low as 450 °C, and a pure perovskite phase was obtained upon calcination at 600 °C. The average particle sizes of PB_xT powders heat-treat at 600 °C were approximately 40–80 nm. The surface areas of the powders ranged from 6.3 m^2/g to 16.6 m^2/g. In addition, the phase transition from the tetragonal ferroelectric phase to the cubic paraelectric phase occurred at $0.6 < x < 0.8$.

Acknowledgement

The authors gratefully acknowledge the financial support of the National Science Council of the Republic of China (Taiwan).

References

[1] D. Bao, X. Wu, L. Zhang, X. Yao, Thin Solid Films 350 (1999) 30.
[2] P. Kumar, S. Singh, M. Spah, J.K. Juneja, C. Prakash, K.K. Raina, Journal of Alloys and Compounds 489 (2010) 59.
[3] H.B. Sharma, H.N.K. Sarma, A. Mansingh, Journal of Materials Science 34 (1999) 1385.
[4] A. Garg, D.C. Agrawal, Materials Science and Engineering B86 (2001) 134.
[5] S. Chopra, A.K. Tripathi, T.C. Goel, R.G. Mendiratta, Materials Science and Engineering B100 (2003) 180.
[6] J.F. Meng, R.S. Katiyar, G.T. Zou, Journal of Physics and Chemistry of Solids 59 (1998) 1161.
[7] P.T. Diallo, K. Jeanlouis, P. Boutinaud, R. Mahiou, J.C. Cousseins, Journal of Alloys and Compounds 323–324 (2001) 218.
[8] W. Liu, W. Zhu, Materials Letters 46 (2000) 239.
[9] D. Liu, H. Zhang, Z. Wang, L. Zhao, Journal of Materials Research 15 (2000) 1336.
[10] S.W. Boland, S.C. Pillai, W.-D. Yang, S.M. Haile, Journal of Materials Research 19 (2004) 1492.
[11] W.D. Yang, S.M. Haile, Thin Solid Films 510 (2006) 55.
[12] N.V. Giridharan, R. Jayavel, Materials Letters 52 (2002) 57.
[13] W.-D. Yang, S.M. Haile, Journal of the European Ceramic Society 25 (2006) 3611.

[14] F.M Pontes, M.S. Galhiane, L.S. Santos, R.S. Rissato, D.S.L. Pontes, E. Longo, E.R. Leite, P.S. Pizani, A.J. Chiquito, M.A.C. Machado, Materials Chemistry and Physics 108 (2008) 312.
[15] M. AlguerÓ, M.L. Calzada, C. Quintana, L. Pardo, Applied Physics A68 (1999) 583.
[16] S. Doeuff, M. Henry, C. Sanchez, J. Livage, Journal of Non-Crystalline Solids 89 (1987) 206.
[17] T. Yoko, K. Kamiya, K. Tanaka, Journal of Materials Science 25 (1990) 3922.
[18] C. Lemoine, B. Gilbert, B. Michaux, J.-P. Pirard, A. Lecloux, Journal of Non-Crystalline Solids 175 (1994) 1.
[19] K.-M. Hung, W.-D. Yang, C.-C. Huang, Journal of the European Ceramic Society 23 (2003) 1901.
[20] M.H Frey, D.A. Payne, Chemistry of Materials 7 (1995) 123.
[21] B. Malic, N. Setter, K. Brooks, M. Kosec, G. Drazic, Journal of Sol–Gel Science and Technology 13 (1998) 833.